Lasers in Manufacturing Conference 2021

Towards optimization of femtosecond laser pulse nano-structuring for high-intensity laser matter interactions

Ulrich Teubner[a,b,*], Jürgen Imgrunt[a] , Alexander Andreev[a,c]

[a]*Institut für Laser und Optik, Hochschule Emden/Leer – University of Applied Sciences, Constantiaplatz 4, 26723 Emden, Germany*
[b]*Institut für Physik, Carl von Ossietzky Universität Oldenburg, Ammerländer Heerstr. 114-118, 26111 Oldenburg, Germany*
[c]*Saint-Petersburg State University, 199034 Universitetskaya Emb. 7-9, St. Petersburg, Russia*

Abstract

The interaction of intense femtosecond laser pulses with solid targets is a topic that has attracted large interest in science and applications. For many of the related experiments a large energy deposition or absorption and an efficient coupling to EUV- (extreme ultra violet, sometimes termed instead XUV) and/or X-ray photons and/or high energy particles is important. Here, beside improvements in laser pulse properties also those of the target are relevant. The present work investigates the formation of laser-induced periodic surface structures on massive metal targets by femtosecond laser pulses in vacuum. The experimental results and the ripple formation mechanisms have been analysed and interpreted with theoretical models. The present results contribute to a simple optimization of targets by nano-structuring their surface *in-situ* which leads to a significantly enhanced absorption and conversion efficiency into EUV emission, X-rays and/or high energy electrons and protons after irradiation with a subsequent intense laser pulse.

Keywords: LIPSS, ripple, high intensity femtosecond pulse, X-ray, EUV, XUV, high energy particles, proton acceleration

1. Introduction and motivation

After extensive investigations of laser-produced plasmas (LPP) in general in the 1990's and further progress of related research within this century, the emission of LPP has found wide-spread applications. Furthermore advances in laser technology make it possible that even with relative small fs and ps laser systems significant X-ray or extreme ultraviolet (EUV) emission can be achieved which then is applicable, e.g., for EUV lithography, time resolved X-ray diffraction, tests of EUV- and X-ray optics, (gated) medical imaging, biological experiments and much more. Moreover, LPP can be used as sources of high energy electrons, protons or ions. Here, in particular, beside other applications, such a proton or ion source is of large interest for tumor therapy.

For all those applications optimization of the LPP source is important. Consequently, there are a lot of investigations on that subject where the emission is boosted by the increase of laser intensity *I* (but note, dependent on the particular application, not necessarily a larger *I* leads to an increased amount of X-rays or particles), the optimization of the target and its geometry (including target material, angle of incidence etc.), the application of well defined pre-pulses and so on (see, e.g. Teubner, Kühnle and Schäfer, 1991; Teubner et. al, 1993; Teubner et. al, 1995; Teubner, Theobald and Wülker, 1996; Altenbernd et al., 1997, just to mention a few of the own results).

Another topic is the optimization of the target itself, in particular, the conditioning of its surface. This is the topic of the present work. As an example of the most simple conditioning, Fig.1 displays 6 spectra from a LPP when the laser pulse is always focused on the same spot on the target. It is well seen that the emission of the 1st shot which hits a plane polished target is significantly smaller when compared too the following ones which are focused to the craters of the previous shots. Due to the rough surface, the absorption is increased and thus the plasma emission as well. Only after the 5th shot the crater becomes so deep, that the emission is strongly reduced. If, in contrast, the target is moved after each shot, the spectra are well reproducible (not shown here).

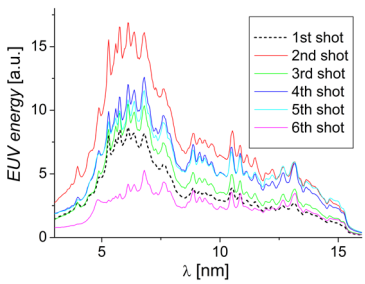

Fig. 1. EUV emission of a sub-fs Aluminum LPP ($I = 2 \cdot 10^{16}$ W/cm^2, pulse duration 400 fs). Six single-shot spectra originating of consecutive shots irradiated on the same spot.

However, such a procedure is neither well defined nor optimized for the LPP emission. Hence, alternatively targets with a structured surface can be used. In particular, very accurate and well reproducible surface patterning can be achieved by direct laser writing. Some examples of the own group are presented in Fig.2 (structured with the laser system described in section 2). But although targets with such structures may be applied, the disadvantage is that some effort is necessary for surface conditioning and this cannot be done *in-situ*. Furthermore, the application of this kind of micro structures is restricted to large LPP (large laser spots in the focus) and not necessarily the ratio of the laser wavelength λ_L to the structure size is optimized for an increased absorption and an enhanced coupling. Consequently another approach becomes necessary to reach the present goal of an improved coupling. This is discussed in the following.

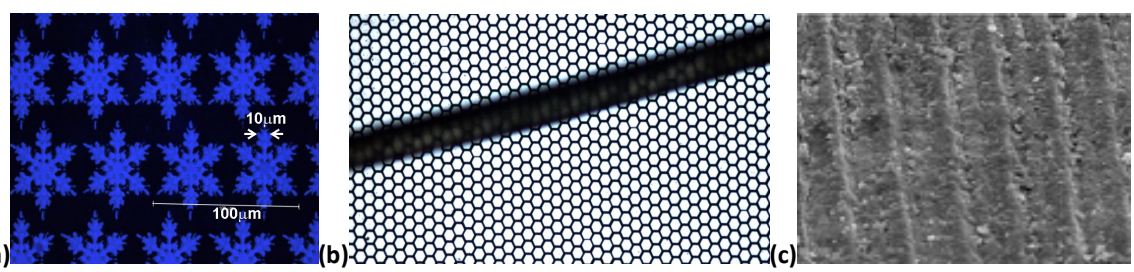

Fig. 2. Examples of fs-laser machined surfaces structures (image crops). (a) Snowflake pattern. (b) Structured photo electrode for thin film photovoltaics (for comparison: the dark stripe is a human hair; the width of an individual cell is 20 μm). (c) Target for proton acceleration experiments with 10 μm interline spacing (work performed in collaboration with S. Huber and M. Schnürer).

2. Experimental setup

More recently, a different approach, namely patterning by laser induced periodic surface structures (LIPSS) has been suggested to achieve higher absorption, conversion efficiency and electromagnetic or particle emission (Lübcke et al., 2017). This method has the advantage to be rather simple and it can be applied *in-situ* in a well defined way. Fig.3 shows the scheme. First the initially flat target surface is nano-structured by the irradiation with tens of pulses (displayed in purple colour) with much reduced intensity (in the following we will call this "*formation pulses*"). Then, second, the main laser pulse will arrive (red colour) and hit the ripple profile on the surface at exactly the same position but with full intensity. Typically all these pulses have a Gaussian shape. If the ripples (i.e. LIPSS) are optimized, absorption, conversion efficiency into fast particles and hard X-ray photons or into soft X-rays and/or EUV emission during the interaction with the main pulse is significantly enhanced when compared to plane targets (in the following we will call this "*main pulse*" interaction). We may mention that the laser pulse must not be irradiated at normal incidence as this depends on the application. For instance for soft X-rays and/or EUV emission intermediate angles of incidence are preferable (Teubner et. al, 1995), whereas proton acceleration experiments often are carried out at angles between 0° and 30° (Daido, Nishiuchi and Pirozhko, 2012; Fuchs et al., 2006).

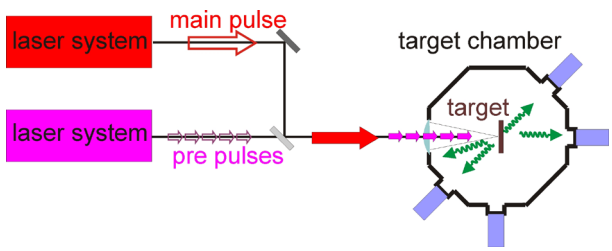

Fig. 3. Scheme of *in-situ* LIPSS generation within high-intensity laser plasma experiments. The pre-pulses may be generated by the same laser as the main pulse. The displayed separation of both systems is made just for a more clear description. Usually both, pre-pulses and main pulse, will originate from the same system, however at much different repetition rates (pre-pulses at kHz, main pulse typically up to 10 Hz). The target emission (photons, electrons, protons and/or ions, here not discriminated) is shown in green colour, the diagnostics or the application set-up is indicated by the blue boxes. Note, that in real experiments focusing is not necessarily performed by a simple single lens as shown in this scheme, but with a more complex optical system and often with focusing mirrors.

In general, LIPSS has attracted strong interest in laser micromachining. LIPSS formation is largely attributed to the interference of the incident laser wave and the surface scattered electromagnetic wave, thus creating a periodic pattern along the irradiated surface (Bonse et al., 2012). For the particular background we refer to the literature (see, e.g. Sipe et al., 1983; Sugioka and Cheng, 2013; Bonse et al., 2017).

However, although a lot of investigations have been reported on that subject, its special application to enhance the emission of LPP is rather new. In our recent work (Das et al., 2016), the first results on the formation of LIPSS covering extended areas of thin Cu-foil surfaces with the second harmonic of a 120-fs Ti:sapphire laser was discussed. The present work continues the investigation of LIPSS formation on polished massive copper targets but in another parameter range and, in particular, in vacuum. The latter is essential because experiments performed at atmospheric pressure in air (or other gases or gas mixtures) may be strongly affected by chemical reactions whereas in vacuum this does not happen. Indeed SEM images from the present work performed in air and vacuum, respectively, clearly show strong differences (see Fig.4): whereas in vacuum there is a very sharp boundary between the ripple region and the unaffected region (this remains fully flat), in air the boundary is less sharp and outside the corresponding region further ripples were observed. Moreover those "supplementary ripples" have a slightly shifted spatial frequency

(1.33 periods/μm when compared to 1.52 periods/μm in vaccum) and additionally a high frequency component (2.8 periods/μm). Here the measurements in air were made for comparison only. As additional effects induced by air environment are not the subject of the present work, we will not consider that further.

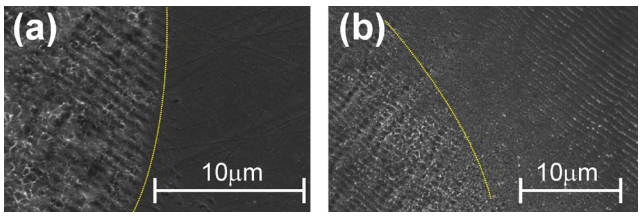

Fig. 4. Crop of SEM images of ripples generated in vacuum (a) and air at atmospheric pressure (b), respectively. The yellow line marks the boundary of the ripple region in vacuum (a) and discriminates the region with the same ripples (as in (a)) from other ones (b). In both cases the peak fluence was F_0 = ~1.5J/cm^2 and the number of shots N = 120. For both images the central peak of the laser pulse is located at the left hand side.

The present experiments were performed at well defined conditions in a vacuum chamber evacuated to 10^{-4} mbar. Plane polished Cu targets were irradiated at normal incidence with τ_L = 153 fs (FWHM) linearly polarized pulses of a Ti:sapphire laser microsructuring system, which is a much advanced version of that described in Imgrunt et al., 2017. The wavelength was λ_L = 775 nm and the maximum applied peak intensity $I_{0,max} \approx 10^{13}$ W/cm^2. The repetition rate was 1 kHz. The slightly elliptical Gaussian shaped focal spot was carefully examined with a beam profiler system yielding a length of d_{ma} = (95 ± 5) μm and d_{mi} = (75 ± 5) μm for the major and minor axis, respectively (1/e^2-width). The dependence of the ripple period λ_r and height h has been investigated for different peak fluences F_0 and as a function of shot number N on the same surface position. Due to our own preliminary experiments the range of N was fixed to a range of 40 to 120 or even 200 for low fluence shots.

Moreover, using the well established and widely used method for threshold determination for pulses with a well-known spatial laser fluence distribution, the threshold for ripple formation F_{th} and that for damage F_d (ablation threshold), respectively, was determined from the diameter of the ripple region (note: the boundary to the unaffected region is very sharp, see Fig.4) and that of the damage crater, respectively, for all different values of F_0 and N.

To provide clear and well defined experimental conditions, the sample was shifted to a new position with an unaffected surface after each series. While keeping the target always at the same focal position, the fluence was changed by changing the laser energy by means of attenuation filters. In that way the fluence at the central peak of the laser pulse was changed between $F_0 = 0.5$ J/cm^2 and 1.5 J/cm^2. After irradiation the sample was cleaned in an ultrasonic bath and then examined by means an optical light microscope, an atomic force microscope and a scanning electron microscope.

3. Experimental results and discussion

3.1. Ripple formation

Fig.5 shows images of ripples obtained with a peak fluence below and above the damage threshold of $F_d(N = 100) = 0.8$ J/cm^2, respectively. The orientation of the wave-vector of the ripples is almost parallel to the laser polarization. From Fig.5(a) it may be well seen that the ripples are rather homogenous and located within an slight ellipse which results from the corresponding laser profile. In contrast to this, when the fluence exceeds the damage threshold, an ablation crater is apparent in the centre of the spot with a ring-shaped ripple region around (Fig.5(b)). Of course such a situation is in contradiction to the goal of the

present work where a potential main pulse is intended to be focused on a rather homogenous ripple area within the vicinity of the spot centre. Consequently situations for ripple generation with $F_0 > F_d$ will not considered further in the following.

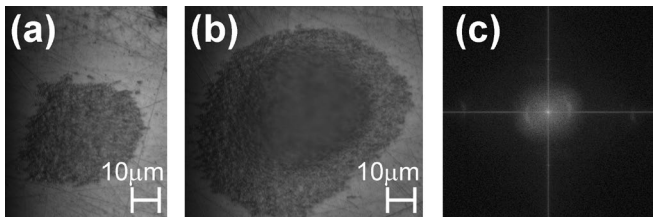

Fig. 5. Images of ripples generated with N = 100 shots on a Cu target located in vacuum. (a) $F_0 = 0.75$ J/cm² < F_d and (b) $F_0 = 1.45$ J/cm² > F_d. (c) Fourier spectrum of the ripples displayed in (a). Here the spatial frequency is 1.55 periods/μm which corresponds to a ripple period of $\lambda_r \approx 645$ nm.

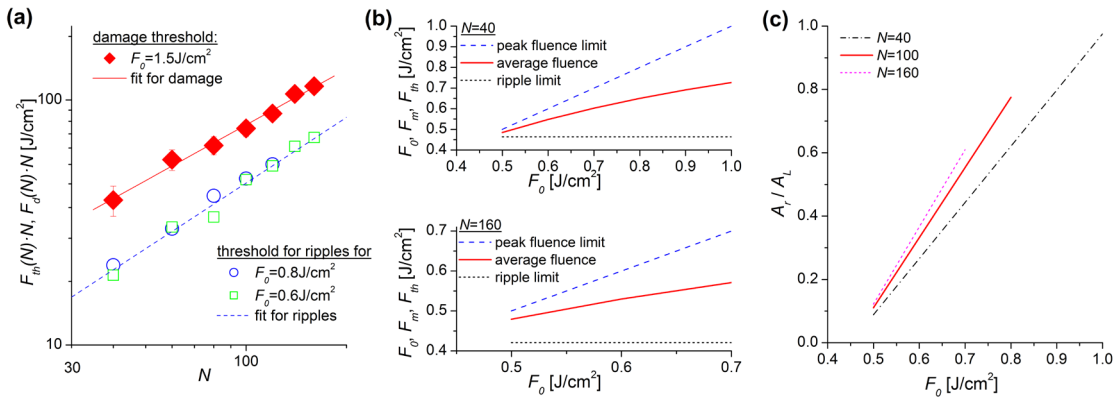

Fig. 6. (a) Accumulated fluence threshold for ripple generation and damage respectively, as a function of the number of shots. (b) Average fluence F_m in the ripple area A_r, where F_m is the energy supplied within A_r divided by A_r. A_r is calculated from the threshold values deduced from (a). (c) Relative area covered by ripples (with respect to the FWHM laser spot area) as a function of F_0. The lines in (b) and (c) have been stopped when F_0 reaches the damage threshold.

Fig.6(a) presents the accumulated fluence thresholds for ripple generation $F_{th} \cdot N$ and damage $F_d \cdot N$ respectively. The peak fluences for the corresponding measurements are indicated in the insert. For the damage measurements, of course, $F_0 > F_d$ whereas for the ripple measurements the peak fluence was set below damage threshold. For ripple formation the results do not show a significant difference for measurements performed at different values of F_0. Independent of F_0 one may fit the data according to a power law

$$F_d(N) = F_{d1} \cdot N^{\Gamma_d} \qquad (1)$$

$$F_{th}(N) = F_{r1} \cdot N^{\Gamma_r} \qquad (2)$$

where F_{r1} = 0.6 J/cm² and F_{d1} = 2.0 J/cm² are the single-shot thresholds and Γ_r = -0.07 and Γ_d = -0.2 are the corresponding scaling coefficients. Eq.(1) is the typical result of incubation effects as observed for ns- (Jee, Becker and Walser, 1988) and fs-pulses (see, e.g. Byskov-Nielsen et al., 2010), respectively. As expected, the phenomenological scaling of eq.(2) indicates that ripple formation is a multiple shot effect, where

subsequent pulses find a surface that is nano-structured by the previous ones. This improves the absorption and lowers the formation threshold. Similar results have been discussed by other groups (see, e.g. Sugioka and Cheng, 2013 and references therein, Bonse et al., 2017 and references therein, Lübcke et al., 2017; Volkov et al.; 2003 Zuhlke et al., 2018).

For the present conditions, where the applied intensity of the ripple formation pulses is rather high, the plasma formation threshold is well exceeded. Consequently plasma physics plays a major role. Hence ripple formation can be well described by parametric processes involving surface plasma waves (see, e.g., Sakabe et al., 2009 and references therein).

Briefly, the idea of that model is the following. First, a femtosecond laser pulse induces a plasma surface wave. Then during its propagation ions become enriched locally and thus experience a strong Coulomb repulsion until the peak of the next electron wave arrives at that position. Second, those spatially localized ion clouds lead to Coulomb explosion and to expansion to vacuum. Third, a thin layer is ablated thus giving rise to the formation of periodic grating structures, which can be regarded as an imprint of a "grating" according to the interspacing of the regions where Coulomb-explosion and thus ablation occurs. If the fluence is large enough, once such structures are formed by the first pulses of a pulse train, an enhancement process takes place for the subsequent pulses within the pulse sequence. The electric field is enhanced near the initially imprinted structures, and the strong near field leads to further ablation of the surface, which results in further deepening of the structures. Within such a model ripple formation could be well described analytically and numerically. Details are discussed elsewhere (Andreev et al., 2021). In particular, as a result the ripple period is obtained as a function of F_0 and N

$$\lambda_r \approx 1.15 \cdot \lambda_L \left(\frac{F_0}{F_A N} \right)^{0.1} \qquad (3)$$

where $F_A \approx 0.2$ J/cm^2 is the absorbed energy (in average). This is in good agreement with the experimental results where the ripple periods were deduced from the Fourier spectra such as that displayed in Fig.5(c) (further experimentally deduced $\lambda_r(F_0,N)$ data are presented elsewhere (Andreev et al., 2021)). Eq.(3) shows that the dependence on the peak fluence is rather small. This is well understandable if one considers the fluence within that region where ripples are generated. This is displayed in Fig.6(b) which results of a calculation based on the experimental data for two different applied number of shots. Within the ripple region the fluence range is limited by F_{th} (lower limit) and F_0 (upper limit; note that here always $F_0 < F_d$), respectively. F_{th} is a function of N. Consequently the average fluence F_m within this region cannot change too much, particularly when damage has to be avoided.

3.2. Relevance for the optimization of the EUV, X-ray and particle emission

Fig.6(c) shows how the ripple area A_r increases with the increase of peak fluence. Intentionally the calculation was stopped when the F_0 becomes equal to $F_d(N)$. It is well seen, that when the peak fluence comes close to the damage threshold, A_r coves a significant fraction of the area taken by the FWHM of the laser spot A_L. In particular, for large N the ripple region fills almost A_L. The central region with A_L is the most important region for the considered laser matter interaction, as the ultrashort plasma emission in the EUV or X-ray region, respectively, and also the high energy particle generation base on the high intensity which is mostly centred in the vicinity close to the peak, namely within the FWHM (or less) of the laser intensity distribution in the focus (here we disregard the rather long lasting emission from the cooling plasma which takes ns). Even more, this is the case as many of the related processes are non-linear.

For that reason it is advantageous to have approximately 100 to 160 pre-pulses prior to the main pulse (see Fig.3). On the other hand an efficient LPP particle source (EUV or X-ray photons, high energy electrons or protons) requires additionally an optimized ripple profile (note the optimized conditions for photons, electrons or protons must not be the same).

For instance a theoretical analysis of laser particle acceleration (Andreev et al., 2016) performed for flat and structured Cu targets, respectively has shown that a triangle-shaped ripple profile with a base between 300 and 350 nm and a height of $h_r \approx 50$ to 100 nm is well suitable (ideally $h_r \approx \lambda_r$ (Margarone et al., 2012; Zigler et al., 2013). From the experimental results obtained from the present experiments, such a profile could be produced with approximately $N = 100$ pulses with a peak fluence of $F_0 \approx 0.8$ J/cm^2 (the corresponding peak intensity is $I_0 \approx 4 \cdot 10^{12}$ W/cm^2; with 80% of the pulse energy within the 150 fs FWHM). For those conditions the present AFM measurements showed a triangular shaped surface structure with $\lambda_r \approx 650$ nm and $h_r \approx 100$ nm and a diameter of the ripple region which almost covers the laser spot. This is consistent with the end of the red solid line in Fig.6(c), in other words nearly 80% of A_L is covered by ripples.

Independent theoretical works have shown that such a surface structure will lead to an enhanced absorption (60 to nearly 100%) and an improved coupling to the emission (Andreev et al., 2011a; Andreev et al., 2019). Likewise, it was shown that as a consequence the K-α emission could be boosted by a factor of 3 (Andreev et al., 2011b), the number of high-energy electrons by a factor of 5 and that of the high-energy protons by a factor 7 (Andreev et al., 2019). However, we would like to note that the optimization with respect to, e.g., EUV or soft X-ray emission, K-α emission or to protons, respectively, is not the same. The EUV or soft X-ray emission requires an optimal heated plasma with high density and the K-α emission requires the generation of a large number of electrons with an energy approximately 2 to 3 times larger than that of the K-α transition (i.e. an optimization with respect to the K-shell ionization cross section). In contrast to that the process of proton acceleration is different (mostly target normal sheath acceleration, TNSA (Daido, Nishiuchi and Pirozhko, 2012; Andreev et al., 2019)).

Thus, dependent on the desired emission, in addition to the present target optimization, this sets requirements to the main laser pulse and the interaction set-up in general. But that is not a subject of the present work which is related to the *pre-pulse interaction* and not to the *main pulse interaction*.

4. Summary

In summary we have investigated ripple formation on flat Cu targets initiated with intense 150 fs laser (ripple formation) pulses in vacuum. The goal has been to find optimized conditions to generate a nano-structured surface for an improved laser matter interaction with an even more intense subsequent main laser pulse. Moreover, ripple pattern generation should be possible and easily implementable *in-situ* within a more complex arrangement with the major aim to achieve a significantly enhanced absorption and conversion efficiency of the main pulse into EUV emission, X-rays and/or high energy electrons or protons.

The present investigation has demonstrated that this is possible. A train of approximately 100 pulses focused to a peak fluence or intensity close but below the corresponding damage threshold ($F_0 \approx 0.8$ J/cm^2, $I_0 \approx 4 \cdot 10^{12}$ W/cm^2) yields a rather homogenous ripple pattern with a fitting size of the ripple region well suitable to be implemented in such an advanced LPP particle source (photons, electrons, protons). At such conditions an appropriate periodic pattern of (approximately) triangles with a base of about 320 nm and a height of 100 nm can be generated.

A theoretical investigation and simulation performed complementarily is in good agreement with the experimental results. Especially, for the present conditions of intense fs-pulses, plasma physics plays a major role and ripple formation could be described on base of surface plasma waves. According to this description

the present estimates yield analytical scaling laws that are useful for the application of ripple generation within the present goal. If beside the optimization of pre-pulse ripple formation also the main pulse parameters will be optimized for a particular emission (EUV *or* a specific X-ray photon energy *or* protons of a specific energy etc.), then according to simulations performed by other groups one may expect a boost of the emission by a factor of at least 3 to 7. Thus the present work contributes to a significant progress with respect to laser driven emission secondary source efficiencies.

Acknowledgements

The authors would like to thank V. Braun, J. Diekhoff, I. Dittmar and M. Sohn for assistance with the SEM and AFM measurements, respectively. A.A. and U.T are grateful to the Deutscher Akademischer Austauschdienst (DAAD) for support by the DAAD Gastdozentenprogramm, grant no. 57371110.

References

Altenbernd, A., et al., 1997, J. Phys. B **30**, p.3969
Andreev, A., et al., 2011a, Phys. Plasmas **18**, 103103
Andreev*, A.,* Platonov, K. Yu. , 2011b, Quant. El. **41**, p.515
Andreev, A., et al.,2016, Plasma Phys. Control. Fusion **58**, 014038
Andreev, A. et al., 2019, Phys. Plasmas **26**, 113110
Andreev, A. et al., 2021, Appl.Phys.A **127**, p.564
Bonse, J., et al., 2012, J. Laser Appl. **24**, 042006
Bonse, J. et al., 2017, IEEE J.Sel.Top.Quant.El. **23**, 9000615
Byskov-Nielsen, J., et al., 2010, Appl.Phys.A **101**, p.97
Zuhlke, C.A. , et al., 2018, AIP ADVANCES 8, 015212
Das, S. K. , et al., 2016, J. Appl. Phys. **119**, 113101
Daido, H., Nishiuchi, M., Pirozhko, A.S , 2012, Rep. Prog. Phys. **75**, 056401
Fuchs, J., et al., 2006, Nature Physics 2, p.48
Imgrunt, J., et al., 2017, Appl. Phys. A **123**, p.776
Jee, Y., Becker, M.F., Walser, R.M., 1988, J. Opt. Soc. Am. B **5**, p.648
Lübcke, A. , et al., 2017, Sci. Rep. **7**, 44030
Margarone, D., et al., 2012, Phys. Rev. Lett. 109, 23480
Sakabe, S., et al., 2009, Phys. Rev. B **79**, 033409
Sipe, J. E. , et al., 1983, Phys. Rev. B **27**, p. 1141
Sugioka, K., Cheng, Y., (eds), 2013, *Ultrafast Laser Processing*, Pan Stanford Publ., Singapore
Teubner, U. , Kühnle, G., Schäfer, F. P., 1991, Appl. Phys. Lett. **59**, p.2672
Teubner, U. , et. al, 1993, Phys. Rev. Lett. **70**, p.794
Teubner, U. , et. al, 1995, Phys. Plasmas **2,** p. 972
Teubner, U. , Theobald, W., Wülker, 1996, J. Phys. B **29,** p.4333
Volkov, R. V. , et al., 2003, JETP Letters, **77**, p. 473
Zigler, A., et al., 2013, Phys. Rev. Lett. 110, 215004